# General Nanomolding of Ordered Phases

Naijia Liu,[1,*] Yujun Xie,[2,*] Guannan Liu,[1] Sungwoo Sohn,[1] Arindam Raj,[1] Guoxing Han,[3] Bozhao Wu,[3] Judy J. Cha,[1,2] Ze Liu,[3] and Jan Schroers[1,†]

[1]*Department of Mechanical Engineering and Materials Science, Yale University, New Haven, Connecticut 06511, USA*

[2]*Energy Sciences Institute, Yale West Campus, West Haven, Connecticut 06516, USA*

[3]*Department of Engineering Mechanics, School of Civil Engineering, Wuhan University, Wuhan, Hubei 430072, China*

(Received 4 July 2019; published 23 January 2020)

Large-scale, controlled fabrication of ordered phases is challenging at the nanoscale, yet highly demanded as their well-ordered structure and chemistry is the key for advanced functionality. Here, we demonstrate a general nanomolding process of ordered phases based on atomic diffusion. Resulting nanowires are single crystals and maintain their composition and structure throughout their length, which we explain by a self-ordering process originating from their narrow Gibbs free energy. The versatility, control, and precision of this thermomechanical nanomolding method of ordered phases provides new insights into single crystal growth and suggest itself as a technology to enable wide spread usage for nanoscale and quantum devices.

DOI: 10.1103/PhysRevLett.124.036102

Essentially all functional materials including high temperature superconductors [1–3], semiconductors [4,5], ferromagnets [6], plasmonic materials [7], phase change materials [8–10], and topological insulators [11–13] are ordered phases. Ordered phases comprise multiple sublattices that are selectively occupied by different atomic species of the chemical compound. Functional properties are demanded for nanoscale applications, which require controlled nanofabrication of ordered phases. However, most nanofabrication techniques for ordered phases are limited to a specific phase, chemistry, or shape [14–21]. Tremendous effort has been taken in the development of nanofabrication techniques. Among bottom-up fabrication approaches, the chemical vapor deposition growth has been widely used to synthesize various materials successfully on the nanoscale. However, the method is limited to materials that can be readily vaporized and morphology control particularly for high aspect ratios remains challenging [14–17]. Top-down approaches, such as *e*-beam lithography, have been developed to fabricate optical, electronic, and metamaterial devices, albeit not suited for large-scale nanomanufacturing [18–21]. Widespread technological exploration and implementation requires a nanoscale fabrication method that is facile, scalable, precise, and broadly applicable to a wide range of ordered phases.

A highly versatile and widely used fabrication method is molding, which is generally associated with a soft state of a material. Nanomolding has been realized for polymers, gels, and some glasses that soften at elevated temperatures, but not for crystalline metals that remain hard in their crystalline state [22–24]. Recently, we discovered that nanomolding is possible with some metals and solid solutions [25,26]. However, the composition of the molded nanostructure varied uncontrollably. We thus hypothesized that the process is controlled by atomic diffusion in the kinetic regime, dictated by the various diffusivities of the constituent atoms of the solid solutions. This would prevent nanomolding of ordered phases as they require a precise stoichiometry.

Surprisingly, we find that a broad range of ordered phases can be nanomolded through thermomechanical nanomolding (TMNM). The TMNM process involves pressing down of a bulk ordered phase into a nanomold at processing temperatures well below the melting temperature, $\sim 0.5T_m$ of the ordered phase. Using TMNM, arrays of single-crystalline nanowires with aspect ratios of up to 1000 and diameters down to 10 nm were formed for a wide range of ordered phases of different crystal structures and properties, including superconductors (FeSe, $AuIn_2$), topological crystalline insulators (SnTe), and phase change materials ($Ge_2Sb_2Te_5$, $Sb_2Te_3$). We explain the observed fabrication process by the narrow Gibbs free energy of ordered phases, which forces the growing crystal to self-organize into the precise structure and chemistry of the ordered phase. In contrast to atomic diffusion of solid solutions, in the thermodynamically driven, self-organization of an ordered phase, the faster moving component is thermodynamically prohibited to occupy the sublattice of the slower moving component, hence, maintaining the structural and chemical order.

For TMNM of ordered phases, we use solid feedstock of an ordered phase to fill the nanocavities in a hard mold [Fig. 1(a)(i)]. Molding is carried out at pressures ranging

 

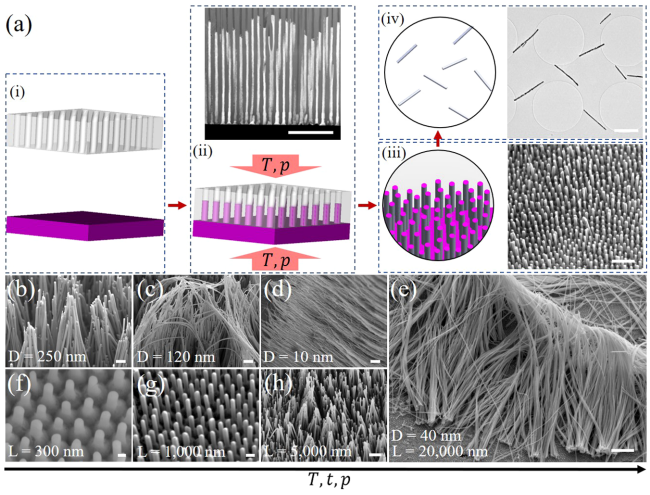


FIG. 1. Thermomechanical nanomolding (TMNM) of ordered phases. (a) For TMNM, (i) a mold composed of nanocavities (e.g., anodic aluminum oxide) and an ordered phase feedstock (typically 0.5 mm thick and 5 mm wide) are prepared. (ii) The mold is pressed against the feedstock at 10–500 MPa and a temperature of $\sim 0.5T_m$ over a time between 1 sec and 1 h. [(ii) top] A cross-section view of the ordered phase nanowires filling the nanocavities of the mold (scale bar: 500 nm). (iii) Subsequently, for large aspect ratios, the mold is chemically etched, leaving behind only the nanowire array of the ordered phase (scale bar: 1 $\mu$m). (iv) Nanowires can be separated from the array by sonication (scale bar: 1 $\mu$m). (b)–(e) $Au_2Al$ nanowires with different diameters: 250, 120, 10, and 40 nm (scale bars: 1 $\mu$m). (e)–(h) $Au_2Al$ nanowires with different lengths: 300 nm, 1, 5, and 20 $\mu$m. The length is controlled by processing temperature, time, or pressure (scale bars: 100 nm, 200 nm, 1 $\mu$m, and 1 $\mu$m).

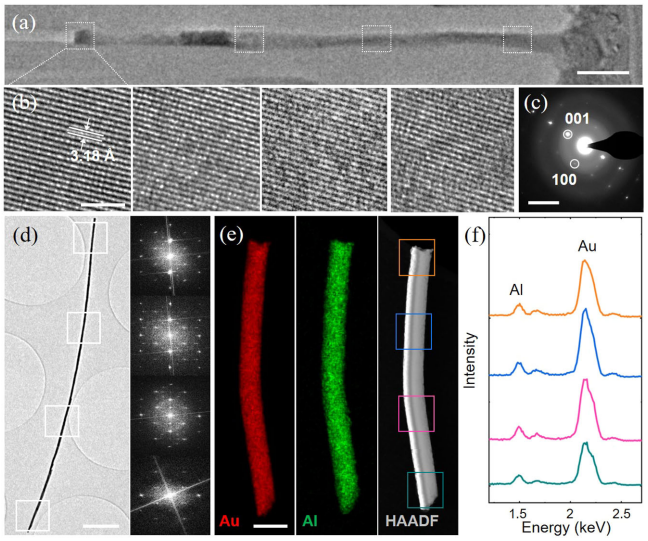


FIG. 2. Ordered phase nanowires as a single crystal, fabricated by TMNM. (a) A SnTe nanowire fabricated by TMNM (aspect ratio ~25, 80 nm diameter and 2 $\mu$m length, scale bar: 200 nm). (b) TEM images from selected regions in (a), showing atomic planes with the same orientation along the entire (scale bar: 2.5 nm). (c) A typical electron diffraction pattern from molded SnTe nanowires, revealing the crystal structure of SnTe viewed from [100] direction (scale bar: 5 $nm^{-1}$). (d) $Au_2Al$ nanowire (aspect ratio >250, 40 nm diameter and 10 $\mu$m length, scale bar: 1 $\mu$m). Diffractograms from high-resolution TEM images (see Supplemental Material, Fig. S7 [27]) from selected regions reveal $Au_2Al$ crystal structure with the same orientation along the nanowire. $Y$ axis of FFT are normalized to growth direction of nanowire. (e),(f) EDS mapping and EDS spectra from the selected regions of the $Au_2Al$ nanowire (diameter 80 nm) reveal the uniform composition along the nanowire, which is identical to the composition of the feedstock (scale bar: 200 nm).

from 10–500 MPa and temperatures of $\sim 0.5T_m$. Molding takes between 1 sec–1 h to produce an array of nanowires with variable and controlled aspect ratios [Fig. 1(a)(ii)]. Demolding of the nanowire array with large aspect ratios is achieved by chemically etching the mold [Fig. 1(a)(iii)]. Individual nanowires of the ordered phase can be obtained through sonication, which separates the nanowires from the feedstock [Fig. 1(a)(iv)].

We use TMNM to fabricate intermetallic $Au_2Al$ nanowires with controllable diameter and length [Figs. 1(b)–1(h)]. The diameter of the nanowires was varied between 10 and 250 nm, as defined by the mold diameter. The length of the nanowires was controlled through the molding parameters; increasing the molding temperature, pressure, and time increases the length of the nanowires. The longest nanowires we fabricated are ~45 $\mu$m in length and 40 nm in diameter (aspect ratio above 1000, see Supplemental Material, Fig. S1 [27]). The length of the nanowires was limited practically by the mold depth we used, and there is no fundamental limit to the length of the nanowire during the TMNM process.

Further characterization of the fabricated nanowires revealed that the nanowires are identical to the ordered phase of the feedstock (Fig. 2 and Figs. S2, S3, S4 in the Supplemental Material [27]). Figure 2 shows transmission electron microscopy (TEM) characterizations of a topological crystalline insulator SnTe nanowire and intermetallic $Au_2Al$ nanowire, fabricated by TMNM. For the SnTe nanowire, high-resolution TEM images from various locations along the nanowire show cubic lattice fringes that look identical to each other [Fig. 2(b)] and the diffraction pattern shows only a single-crystalline grain [Fig. 2(c)]. The single crystallinity of the intermetallic $Au_2Al$ is also confirmed by taking diffraction patterns along the length of the nanowire [Fig. 2(d)]. Thus, for both nanowires, the crystalline orientation remains unchanged throughout the entire length of the nanowire. In addition, chemical analysis along the length of the nanowires by energy dispersive x-ray spectroscopy (EDS) revealed that the composition remains uniform and identical to the composition of the feedstock throughout the nanowire [Fig. 2(e), and more information in Fig. 3(c) and Fig. S3 [27] ]. This finding is in contrast to our previous report of nanomolding of solid solutions, in which the composition varied along the wire

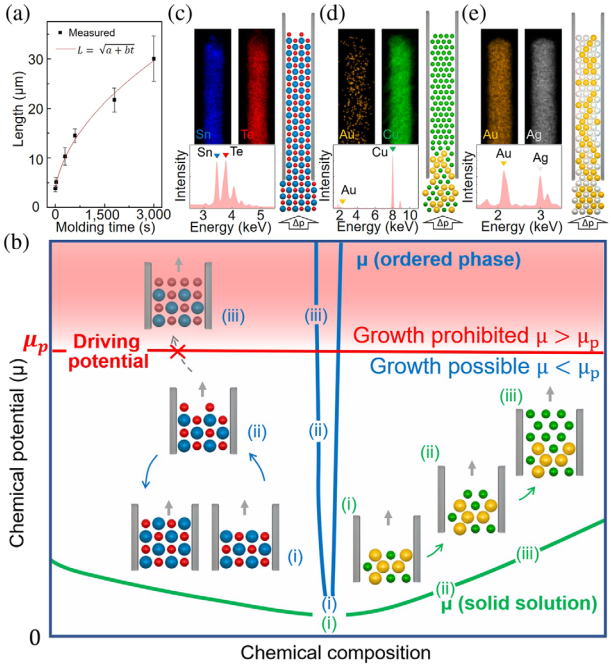


FIG. 3. Atomic mechanism for TMNM of ordered phases. (a) Molding length and molding time exhibit a square root relation, suggesting atomic diffusion as the underlying TMNM mechanism (see Supplemental Material for details [27]). (b) The competition between the lowering of chemical potential due to the reduction of the pressure gradient $\mu_p$ and the energetics associated with the growth of the phase $\mu$ determines if a specific composition can be nanomolded. Specifically, if $\mu_p < \mu$, nanomolding of such a composition is prohibited and if $\mu_p > \mu$, nanomolding is possible. For solid solutions, the growth condition $\mu_p > \mu$ is typically fulfilled over a wide composition range. Therefore, a change in composition of the growing nanorod occurs according to the typically different diffusivities of the alloy's constituents; the small size specie (green sphere) diffuse down the potential gradient faster and hence change the composition of the nanowire. For complete solubility and different diffusivity among the constituents, this can result in a change in composition to entirely that of the faster diffusing constituent [for example in the formation of Cu nanowires when using $Au_{50}Cu_{50}$ as feedstock (d)]. For ordered phases, however, the condition $\mu_p > \mu$ is satisfied only in a very narrow composition range due to their narrow Gibbs free energy curve. Hence, the faster diffusing specie (red sphere) can not occupy the sublattice for the slower specie (blue sphere), as it would increase the chemical potential so that $\mu_p > \mu$ which would prohibit growth thermodynamically (iii). Therefore, TMNM of ordered phases is a self-regulating process to occur only at the specific stoichiometry of the ordered phase. (c)–(e) Composition distribution in nanowires of typical ordered phases SnTe (c), with red sphere representing Te atoms and blue spheres Sn atoms and solid solution (d) $Au_{50}Cu_{50}$, Au orange, Cu green, and (e) $Au_{50}Ag_{50}$, Au orange, Ag white. (c) Ordered phase nanowires (SnTe) with narrow chemical potential show uniform composition, identical to the feedstock material. (d) TMNM of $Au_{50}Cu_{50}$ solid solution with different size components and broad chemical potential result in composition gradient along the nanowire which eventually forms a pure Cu nanowire. (e) However, solid solutions with components of similar diffusivity and broad chemical potential can hold similar composition as feedstock material along the nanowire, for example in the case of $Au_{50}Ag_{50}$.

and can be dramatically different from the composition of the feedstock. The striking finding of this TMNM process is that the structure and chemistry of the ordered phase is realized as a single crystal in the molded nanowires, which is technologically important as single-crystalline ordered phases in the shape of nanowires are often critical requirements for many nanoscale and quantum devices.

The molding of ordered phases into nanowires with large aspect ratios is surprising and was not anticipated from our previous nanomolding results of metals and solid solutions [25,40]. Based on systematic experiments of TMNM of ordered phases as a function of processing time and temperature [Fig. 3(a) and Fig. S5 in the Supplemental Material Fig. S5; see Supplemental Material text for details [27]), we argue that the underlying mechanism for the molding process is atomic diffusion. However, as the diffusivity varies greatly among constituent atoms in compounds or alloys, a kinetically controlled atomic diffusion would dictate the local composition of the forming nanowire during the molding process, resulting in heterogeneous chemical compositions that are outside of the stability range of an ordered phase. Thus, the enabling mechanism for TMNM of an ordered phase cannot be atomic diffusion in the kinetically controlled regime. Instead, we attribute the mechanism to the thermodynamically controlled diffusion regime of self-regulation. For TMNM of nanowires of an ordered phase, two energy terms must be compared for atomic diffusion. One energy term is related to pressure: the driving force for diffusion of atoms to form nanowires in TMNM is, $\Delta p$ the pressure difference between the maximum pressure at the entrance of the mold cavity and the pressure at the tip of nanowire. The chemical potential difference $\mu_p = \Delta p \Omega$, where $\Omega$ represents the average atomic volume, constitutes one thermodynamic term. Diffusion along $\mu_p$ always reduces the Gibbs free energy $G$ of a system. The other is $\mu = \partial G/\partial c$, which describes the change of $G$ with composition $c$ during diffusion. Required conditions for thermodynamically possible nanomolding of ordered phases are $\mu_p > \mu$, where diffusion is dominated by the thermodynamically favored chemical composition that lowers $G$ rather than by the kinetically driven pressure difference.

In an ordered phase, there is one pronounced lowest thermodynamic configuration that leads to the specific arrangement of sublattices occupied by constitute atoms, i.e., $\mu$ is minimum for one specific structure and composition. By contrast, $\mu_p$ does not distinguish between different thermodynamic phases. This is illustrated schematically in Fig. 3(b), which compares $\mu_p$ and $\mu$ of ordered phases and solid solutions. For solid solutions, $\mu$ is small, meaning that the energetics of a phase are not a strong function of composition. Hence, $\mu < \mu_p$ and atomic diffusion leads to an overall decrease of $G$. As $\mu$ does not change significantly with composition for a solid solution, the composition of the nanowire is controlled by atomic diffusion kinetics and is proportional to $D_a/D_b$, where $D_a$ and $D_b$ are diffusivities

of the constituent $A$ and $B$ atoms. This is demonstrated with our attempt to create $Au_{50}Cu_{50}$ nanowires by TMNM [Fig. 3(d)]. $Au_{50}Cu_{50}$ is not an ordered phase but instead a solid solution, and the composition of the nanowire rapidly changes to Cu rich due to the faster diffusion of Cu compared to Au ($D_{Cu} \sim 3.1 \times 10^{-13}$ cm$^2$/s [41], $D_{Au} \sim 1.7 \times 10^{-14}$ cm$^2$/s for $Au_{25}Cu_{75}$ [42]). For kinetically controlled diffusion, if $D_a \approx D_b$, the composition of the nanowire by TMNM should remain constant and identical to the composition of the feedstock solid solution. We tested this hypothesis with $Au_{50}Ag_{50}$ with approximately identical diffusivities ($D_{Au} \sim 1 \times 10^{-14}$ cm$^2$/s and $D_{Ag} \sim 1.6 \times 10^{-14}$ cm$^2$/s [43]). Indeed, we found that throughout the length of the nanowire, the composition remains approximately constant and identical to the nominal composition of the feedstock [Fig. 3(e)]. In contrast to solid solutions, ordered phases have a narrow stable composition range, which originates from the narrow Gibbs free energy curve [Fig. 3(b)]. Hence, nanowire formation of ordered phases by TMNM is only possible in the stochiometric narrow composition range of the ordered phase in order to fulfill $\mu < \mu_p$. Because stoichiometry has to be maintained during TMNM for ordered phases, the atomic diffusion is in the thermodynamically controlled regime and the growth velocity of an ordered phase nanowire is defined by the diffusivity of the slowest diffusing component and insensitive to differences in diffusivities of constituent atoms.

The thermodynamically controlled, self-organizing mechanism should be generally present in ordered phases, suggesting that TMNM can be broadly applied to a wide range of ordered phases to fabricate nanowires of high aspect ratios. The ability to practically nanomold a specific ordered phase can be quantified by the aspect ratio ($L/d$) and its scaling with diffusivity ($D$) [see also Fig. 3(a)]. Using practical fabrication parameters, we generate a map of TMNM of ordered phases, $L/d \propto \sqrt{D}$ [Fig. 4(a) and see Supplemental Material for additional information [27]] ]. The map suggests that ordered phases can be fabricated into nanowires of a high aspect ratio when the diffusivity of the slower species is above $10^{-19}$ m$^2$/s under practical conditions through TMNM. When the diffusivity of the slower species is below $10^{-19}$ m$^2$/s, TMNM is no longer effective. To test the prediction of the TMNM map, we applied TMNM and fabricated a broad range of ordered phases covering different structures and chemistries such as $Ge_2Sb_2Te_5$ (GST), FeSe, $Au_2Al$, SnTe, $Sb_2Te_3$, $Cu_7In_3$, $In_2Bi$, BiSb, $CuAl_2$, $AuAl_2$, $In_{75}Sn_{25}$, AuSn, $AuIn_2$, InBi, $In_{20}Sn_{80}$, InSb, AuIn, Si, and $SiO_2$. They are summarized in Fig. 4(b) (additional systems are in the Supplemental Material, Fig. S6, Table SII and SIII [27]). The considered ordered phases include superconductors (FeSe, $AuIn_2$), topological insulators (SnTe, $Sb_2Te_3$, BiSb), semiconductors (InSb), phase change materials ($Sb_2Te_3$, GST) and colorful alloys ($AuAl_2$). As suggested by the diffusion

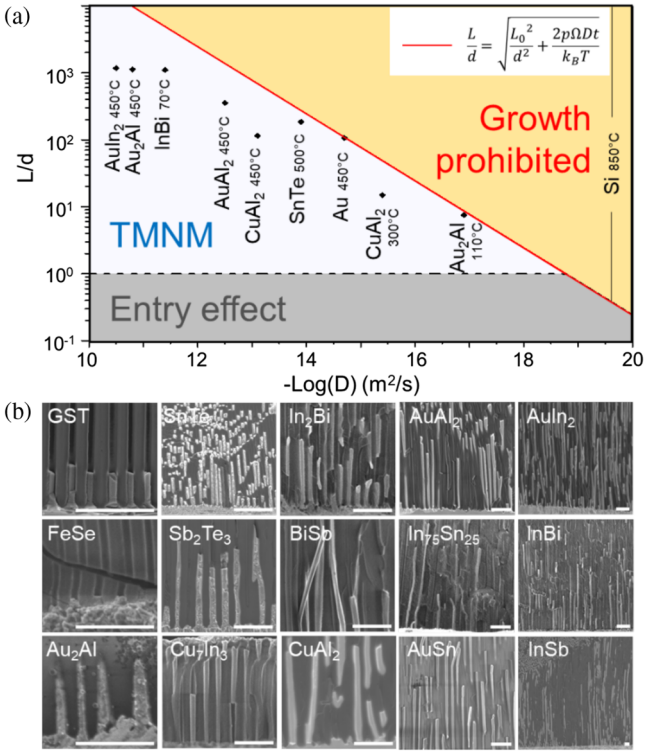


FIG. 4. TMNM map and versatility. (a) TMNM map as a function of diffusivity. Achievable aspect ratios $L/d$, are calculated according to $L/d = \sqrt{(L_0^2/d^2) + (2p\Omega Dt/d^2T)}$, where $L_0$ is the length of nanowires after the pressure ramping, $d$ is the cavity diameter, $p$ is processing pressure, $t$ is time, $T$ is temperature, and $D$ is the diffusivity, assuming practical fabrication parameters (pressure of 400 MPa and processing time of 1 hr, see Supplemental Material for more details [27]). (b) Fabrication of nanowires of ordered phases suggested by the TMNM map. TMNM was successfully applied to fabricate nanowires of $Ge_2Sb_2Te_5$ (GST), FeSe, $Au_2Al$, SnTe, $Sb_2Te_3$, $Cu_7In_3$, $In_2Bi$, BiSb, $CuAl_2$, $AuAl_2$, $In_{75}Sn_{25}$, AuSn, $AuIn_2$, InBi, and InSb with high aspect ratios. The demonstrated ordered phases cover many functional materials including semiconductors (InSb), topological insulators (SnTe, $Sb_2Te_3$, BiSb), superconductors (FeSe, $AuIn_2$), phase change material ($Sb_2Te_3$, GST) and colorful material ($AuAl_2$). Scale bars in (b) are 1 $\mu$m.

growth mechanism, $L/d \propto \sqrt{D}$, ordered phases with $D > 10^{-19} m^2/s$ can be readily fabricated into nanowires with high aspect ratios. On the other hand, silicon ($D = 2.5 \times 10^{-20}$ m$^2$/s) and $SiO_2$ ($D = 7.3 \times 10^{-26}$ m$^2$/s) cannot be fabricated through TMNM into nanowires.

In conclusion, we reveal the underlying mechanism of thermomechanical nanomolding of ordered phases as a thermodynamically self-regulated diffusion transport, enabling precise and predictable fabrication of nanowires of a broad range of ordered phases. As the versatility and control over chemistry, structure, and size of the nanowires possible with TMNM of ordered phases addresses a critical bottleneck in nanofabrication we are looking forward for

a paradigm shift in design and utilization of nano- and quantum devices.

All data are available in the main text or the Supplemental Material [27].

This work was supported by the National Science Foundation through the Advanced Manufacturing Program (CMMI 1901613). N. Liu thanks C. Li for his help when making figures.

The authors declare no competing interests.

*These authors contributed equally to this work.
†Corresponding author.
jan.schroers@yale.edu

[1] J. Paglione and R. L. Greene, Nat. Phys. **6**, 645 (2010).
[2] J. Chen, P. Yu, J. Stenger, M. Hocevar, D. Car, S. R. Plissard, E. P. Bakkers, T. D. Stanescu, and S. M. Frolov, Sci. Adv. **3**, e1701476 (2017).
[3] E. Zhang *et al.*, Nat. Commun. **9**, 4656 (2018).
[4] S. Gazibegovic *et al.*, Nature (London) **548**, 434 (2017).
[5] S. R. Plissard *et al.*, Nat. Nanotechnol. **8**, 859 (2013).
[6] Y. Tao and C. L. Degen, Nat. Commun. **9**, 339 (2018).
[7] Z. Yue, B. Cai, L. Wang, X. Wang, and M. Gu, Sci. Adv. **2**, e1501536 (2016).
[8] F. Rao *et al.*, Science **358**, 1423 (2017).
[9] M. Salinga, B. Kersting, I. Ronneberger, V. P. Jonnalagadda, X. T. Vu, M. Le Gallo, I. Giannopoulos, O. Cojocaru-Mirédin, R. Mazzarello, and A. Sebastian, Nat. Mater. **17**, 681 (2018).
[10] Y. Xie, W. Kim, Y. Kim, S. Kim, J. Gonsalves, M. BrightSky, C. Lam, Y. Zhu, and J. J. Cha, Adv. Mater. **30**, 1705587 (2018).
[11] V. Fatemi, S. Wu, Y. Cao, L. Bretheau, Q. D. Gibson, K. Watanabe, T. Taniguchi, R. J. Cava, and P. Jarillo-Herrero, Science **362**, 926 (2018).
[12] V. S. Pribiag, A. J. Beukman, F. Qu, M. C. Cassidy, C. Charpentier, W. Wegscheider, and L. P. Kouwenhoven, Nat. Nanotechnol. **10**, 593 (2015).
[13] L. A. Jauregui, M. T. Pettes, L. P. Rokhinson, L. Shi, and Y. P. Chen, Nat. Nanotechnol. **11**, 345 (2016).
[14] Y.-C. Chou, K. Hillerich, J. Tersoff, M. Reuter, K. Dick, and F. Ross, Science **343**, 281 (2014).
[15] J. Y. Huang *et al.*, Science **330**, 1515 (2010).
[16] H. Peng, N. Wang, X. Zhou, Y. Zheng, C. Lee, and S. Lee, Chem. Phys. Lett. **359**, 241 (2002).
[17] D. Jacobsson, F. Panciera, J. Tersoff, M. C. Reuter, S. Lehmann, S. Hofmann, K. A. Dick, and F. M. Ross, Nature (London) **531**, 317 (2016).
[18] Y. He, L. Zhong, F. Fan, C. Wang, T. Zhu, and S. X. Mao, Nat. Nanotechnol. **11**, 866 (2016).
[19] D. Jang, X. Li, H. Gao, and J. R. Greer, Nat. Nanotechnol. **7**, 594 (2012).
[20] J. I. Martín, M. Vélez, R. Morales, J. Alameda, J. V. Anguita, F. Briones, and J. Vicent, J. Magn. Magn. Mater. **249**, 156 (2002).
[21] R. G. Hobbs, N. Petkov, and J. D. Holmes, Chem. Mater. **24**, 1975 (2012).
[22] G. Kumar, H. X. Tang, and J. Schroers, Nature (London) **457**, 868 (2009).
[23] H. D. Rowland, W. P. King, J. B. Pethica, and G. L. Cross, Science **322**, 720 (2008).
[24] M. Diez, P. Mela, V. Seshan, M. Möller, and M. C. Lensen, Small **5**, 2756 (2009).
[25] Z. Liu, G. Han, S. Sohn, N. Liu, and J. Schroers, Phys. Rev. Lett. **122**, 036101 (2019).
[26] Z. Liu, Nat. Commun. **8**, 14910 (2017).
[27] See Supplemental Material at http://link.aps.org/supplemental/10.1103/PhysRevLett.124.036102 for details of methods, diffusion model in TMNM, scaling experiments and versatility of TMNM, and additional data, which includes Refs. [28–39].
[28] C. Herring, J. Appl. Phys. **21**, 437 (1950).
[29] R. Balluffi and J. Bkakely, Thin Solid Films **25**, 363 (1975).
[30] R. Fouracre, Thin Solid Films **135**, 189 (1986).
[31] P. Sun and M. Ohring, J. Appl. Phys. **47**, 478 (1976).
[32] H. Hentzell and K. Tu, J. Appl. Phys. **54**, 6929 (1983).
[33] H. Scherrer, G. Pineau, and S. Scherrer, Phys. Lett. **75A**, 118 (1979).
[34] S. Canegallo, V. Agrigento, C. Moraitou, A. Toussimi, L. P. Bicelli, and G. Serravalle, J. Alloys Compd. **234**, 211 (1996).
[35] Y. Hasumi, J. Appl. Phys. **58**, 3081 (1985).
[36] C. Weaver and D. Parkinson, Philos. Mag. **22**, 377 (1970).
[37] D. Gupta and K. Asai, Thin Solid Films **22**, 121 (1974).
[38] T. Südkamp and H. Bracht, Phys. Rev. B **94**, 125208 (2016).
[39] D. Tsoukalas, C. Tsamis, and P. Normand, J. Appl. Phys. **89**, 7809 (2001).
[40] Z. Liu, Phys. Rev. Lett. **122**, 016101 (2019).
[41] F. Lantelme and S. Belaidouni, Electrochim. Acta **26**, 1225 (1981).
[42] D. B. Butrymowicz, J. R. Manning, and M. E. Read, J. Phys. Chem. Ref. Data **3**, 527 (1974).
[43] O. Kubaschewski, Trans. Faraday Soc. **46**, 713 (1950).